Porous P-doped graphitic carbon nitride nanosheets for synergistically enhanced visible-light photocatalytic H_2 production

Jingrun Ran,[a] Tian Yi Ma,[a] Guoping Gao,[b] Xi-Wen Du[c] and Shi Zhang Qiao*[a,c]

[a.] School of Chemical Engineering, The University of Adelaide, Adelaide, SA 5005, Australia.

E-mail: s.qiao@adelaide.edu.au

[b.] School of Chemistry, Physics and Mechanical Engineering Faculty, Queensland University of Technology, Garden Point Campus, QLD 4001, Brisbane, Australia.

[c.] School of Materials Science and Engineering, Tianjin University, Tianjin, 300072, P. R. China.

The calculation of H_2 amount produced in the reactor:

Since the H_2 concentration in the 0.2 mL sample gas is usually assumed to be the same to that in the head space of the reactor, the total amount of H_2 produced in the reactor can be calculated by Equation (1):

$$\text{H2 amount in the reactor [}\mu\text{mol]} = \text{H2 amount in the 0.2 ml sample gas [}\mu\text{mol]} \times \frac{\text{head space volume in the reactor [ml]}}{0.2\ \text{[ml]}} \quad (1)$$

Samples	S_{BET} (m^2 g^{-1})	PV[a] (cm^3 g^{-1})	E_g[b] (eV)	QE at 420 nm (%)
CN-B	5.6	0.03	2.78	0.59
CN-S	84.2	0.23	2.94	2.60
PCN-B	8.3	0.04	2.68	1.50
PCN-S	122.6	0.27	2.91	3.56

[a] PV: Pore volume, [b] E_g: Band gap.

Table S1 Physicochemical properties and QE of CN-B, CN-S, PCN-B and PCN-S

Table S2 Kinetic analysis of emission decay for CN-B, CN-S, PCN-B and PCN-S

Samples	τ_1 (ns)	Rel (%)	τ_2 (ns)	Rel (%)	τ (ns)	χ^2
CN-B	2.885	67.15	15.966	32.85	7.18	1.043
CN-S	3.325	65.10	21.232	34.90	9.58	1.049
PCN-B	3.460	64.10	20.267	35.90	9.49	1.105
PCN-S	3.927	67.60	19.988	32.40	9.13	1.099

Table S3 Parameters of equivalent circuit for the impedance data of CN-B, CN-S, PCN-B and PCN-S

Samples	R_t (Ω)	R_s (Ω)

CN-B	28713	60.7
CN-S	16463	71.4
PCN-B	16627	67.0
PCN-S	8233	64.2

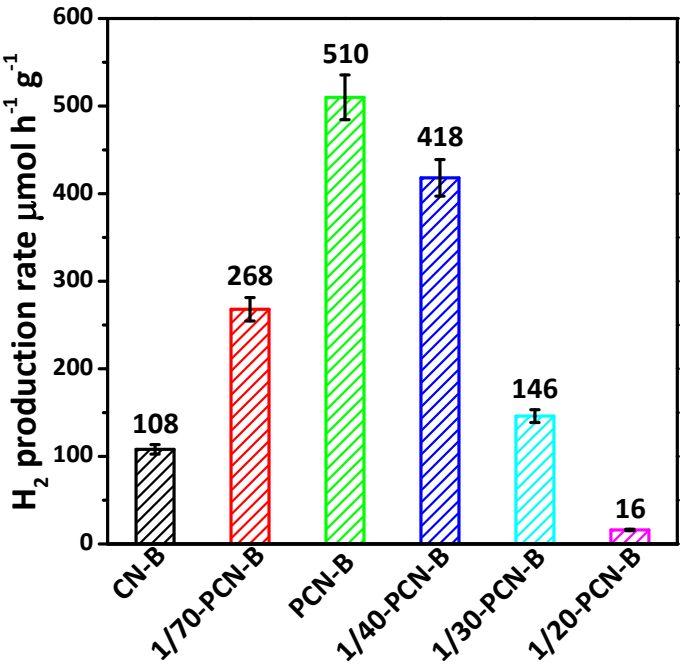

Fig. S1 Comparison of the photocatalytic activities of CN-B, 1/70-PCN-B, PCN-B, 1/40-PCN-B, 1/30-PCN-B and 1/20-PCN-B for the H_2 production using 20 v% TEOA aqueous solution as a sacrificial reagent under visible-light irradiation (≥ 400 nm, 300 W Xe lamp).

In order to determine the optimal doping content of P in g-C_3N_4 for photocatalytic H_2 production, a series of bulk P-doped g-C_3N_4, *i.e.* 1/70-PCN-B, 1/40-PCN-B, 1/30-PCN-B and 1/20-PCN-B were synthesized, following the same procedure as that of PCN-B except that the mass ratio of 2-aminoethylphosphonic acid (AEP):melamine (ME) was changed to 1/70, 1/40, 1/30 and 1/20, respectively. Then the effect of mass ratio (AEP:ME) on the photocatalytic H_2-production activity was investigated. As shown in Fig.

S1, the doping of P in g-C_3N_4 improves the photocatalytic activity towards H_2 production. The photocatalytic H_2-production activity is gradually enhanced as the mass ratio increased and the highest photocatalytic H_2-production activity of 510 μmol h^{-1} g^{-1} is achieved at the mass ratio of 1/60 (PCN-B). However, further increasing the mass ratio leads to the reduction of photocatalytic H_2-production activity. Surprisingly, when the mass ratio reaches 1/20, a very low photocatalytic H_2-production activity of 16 μmol h^{-1} g^{-1} is obtained for 1/20-PCN-B, even much lower than that of undoped g-C_3N_4 (108 μmol h^{-1} g^{1}). On basis of the above result, PCN-B with the optimal mass ratio (AEP:ME) of 1/60 was selected for investigation in this work.

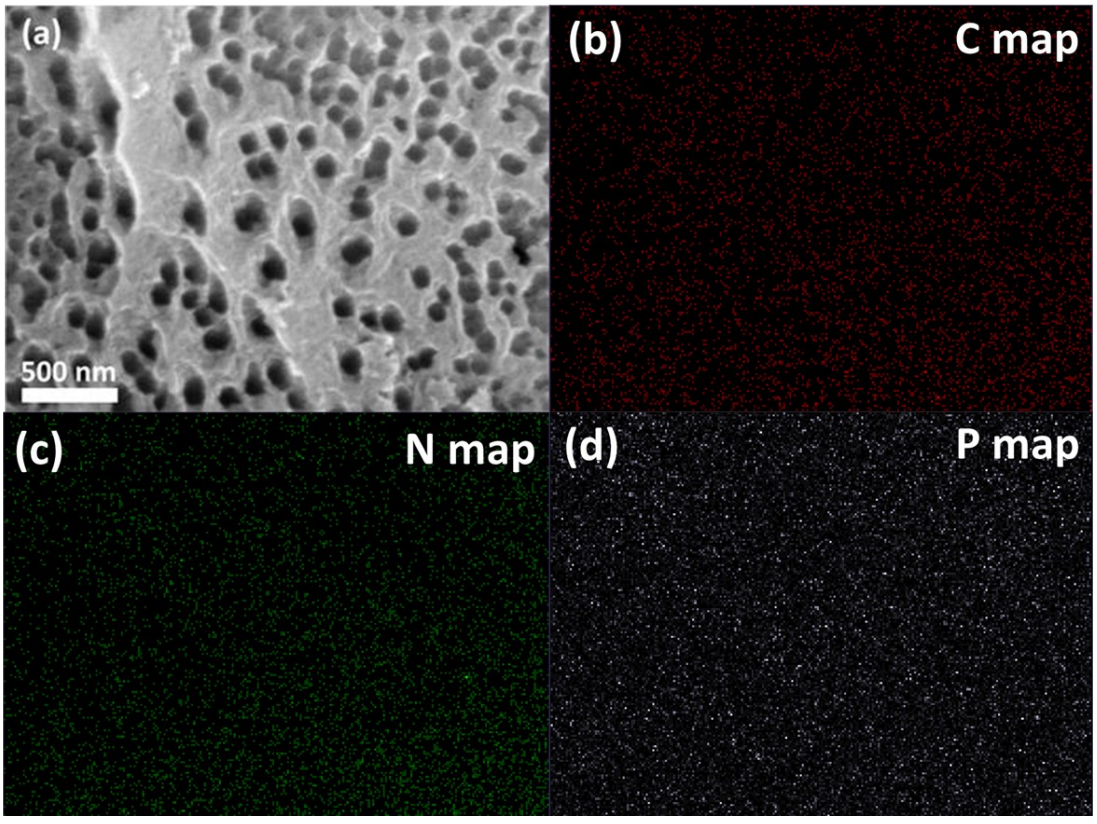

Fig. S2 SEM image (a) of PCN-B and its corresponding EDS elemental mapping images (b-d),

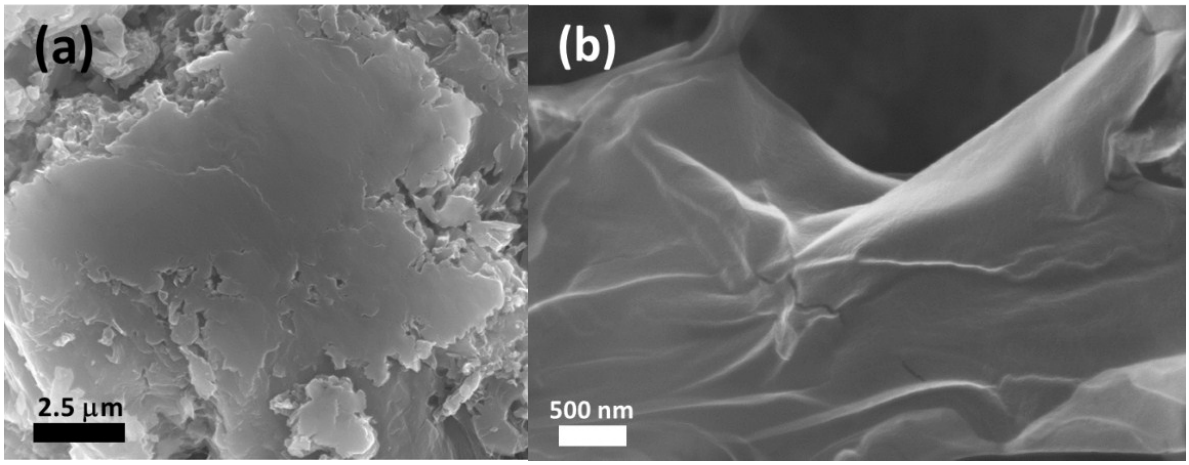

Fig. S3 SEM images of (a) CN-B and (b) CN-S.

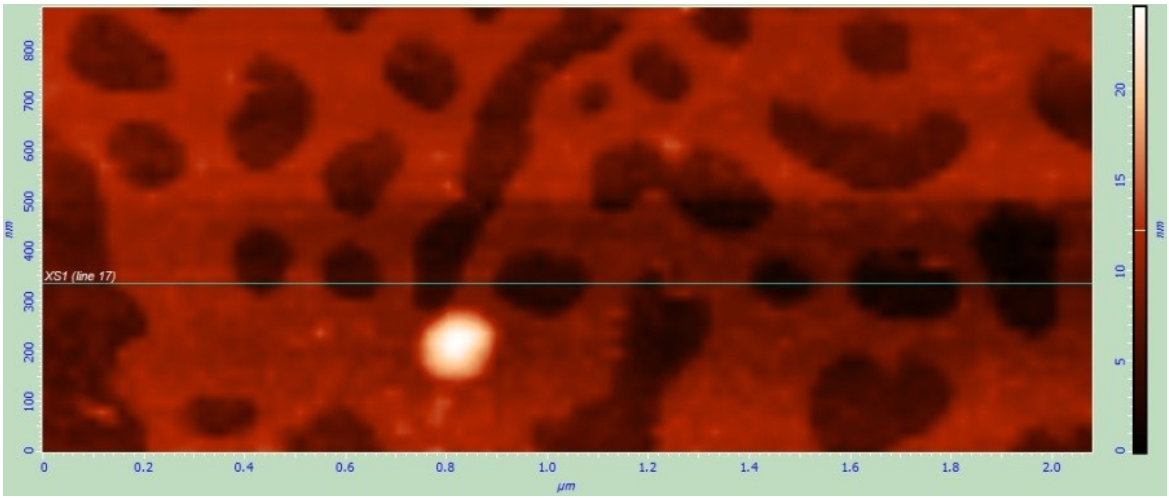

Fig. S4 Original version of the AFM image of PCN-S.

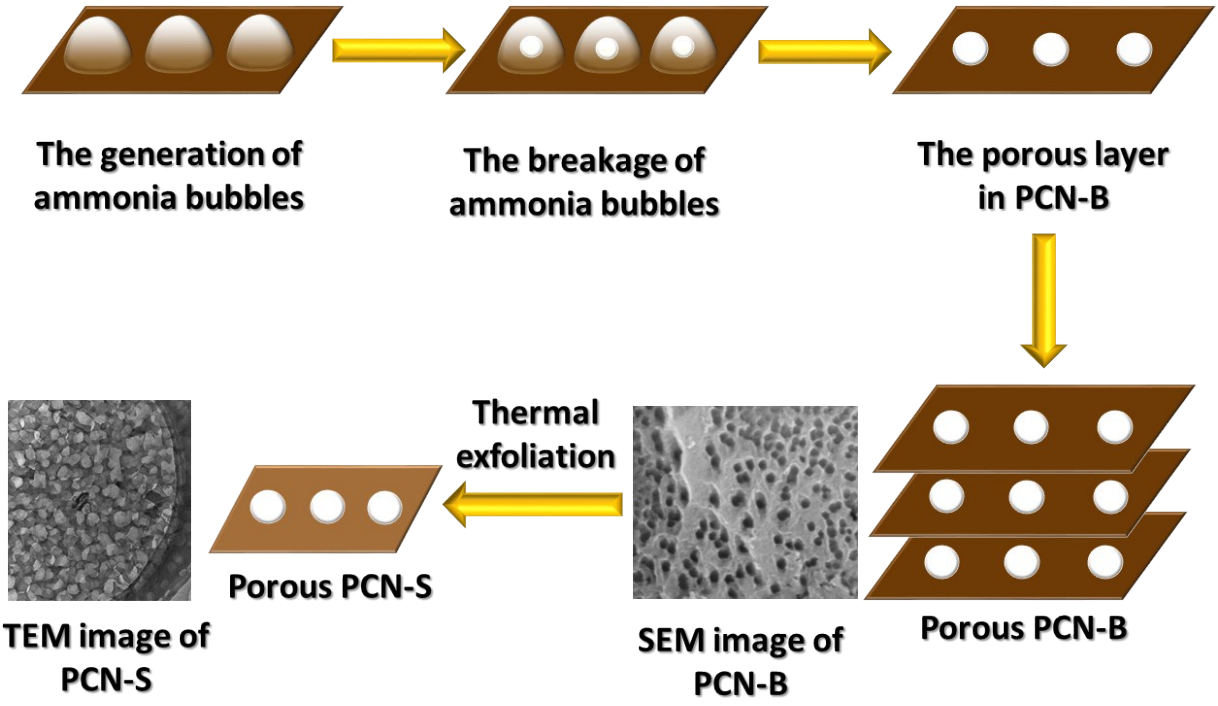

Fig. S5 The pores formation mechanism of PCN-B and PCN-S.

During the thermal poly-condensation, the AEP decomposes to release ammonia bubbles, and their breakage leads to the formation of pores in the layer of PCN-B (The porous morphology of PCN-B is presented in Fig. S2a). Further thermal exfoliation of PCN-B results in the formation of porous nanosheets structure of PCN-S as shown in Fig. 1a. Moreover, due to the random bubbles generation and pores formation, both PCN-B and PCN-S exhibit a broad pore size distribution, as displayed in Fig. 1b.

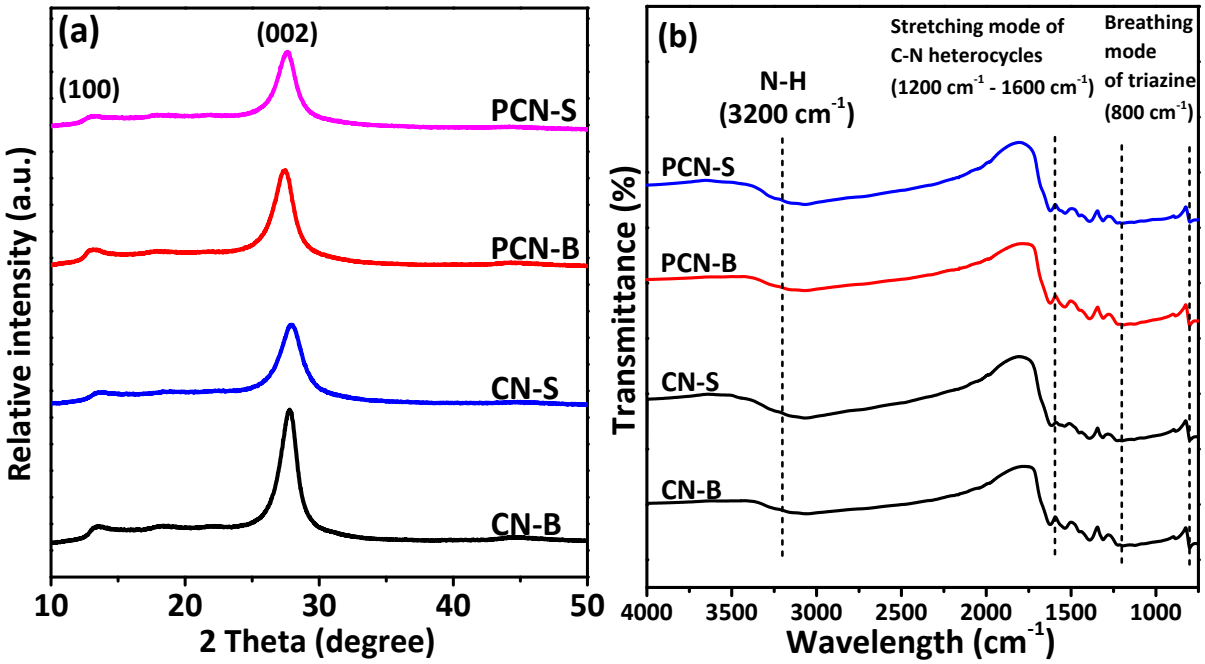

Fig. S6 (a) XRD patterns and (b) FT-IR spectra of CN-B, CN-S, PCN-B and PCN-S.

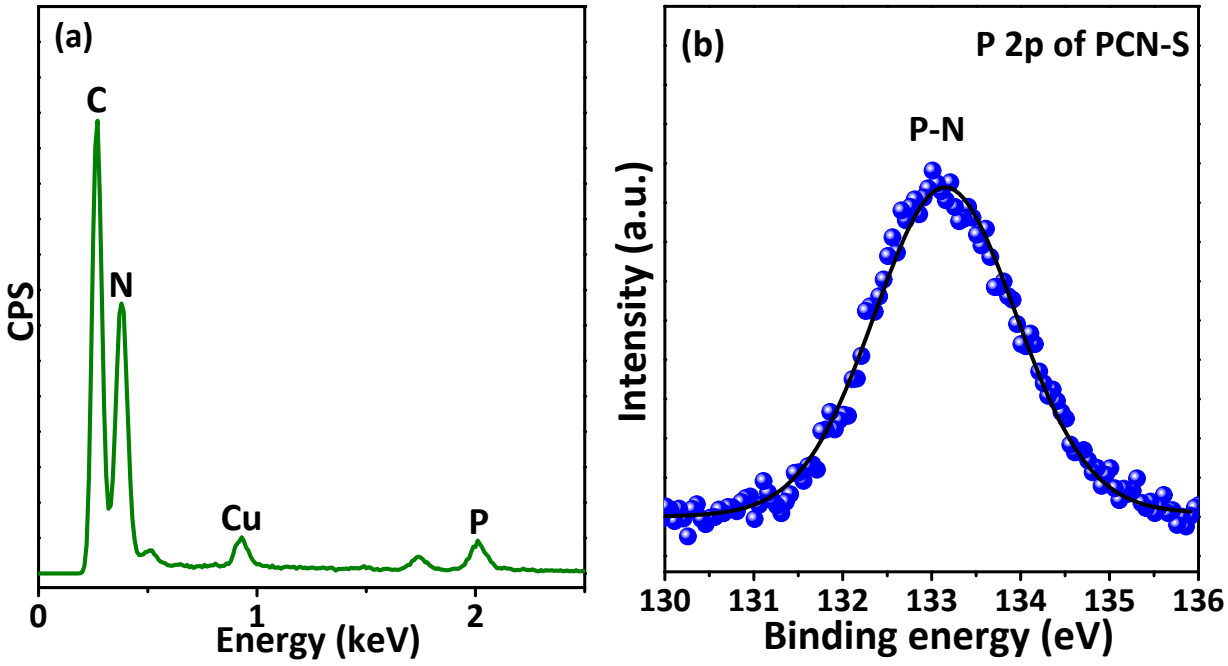

Fig. S7 (a) EDX pattern and (b) high-resolution P 2p XPS spectrum of PCN-S.

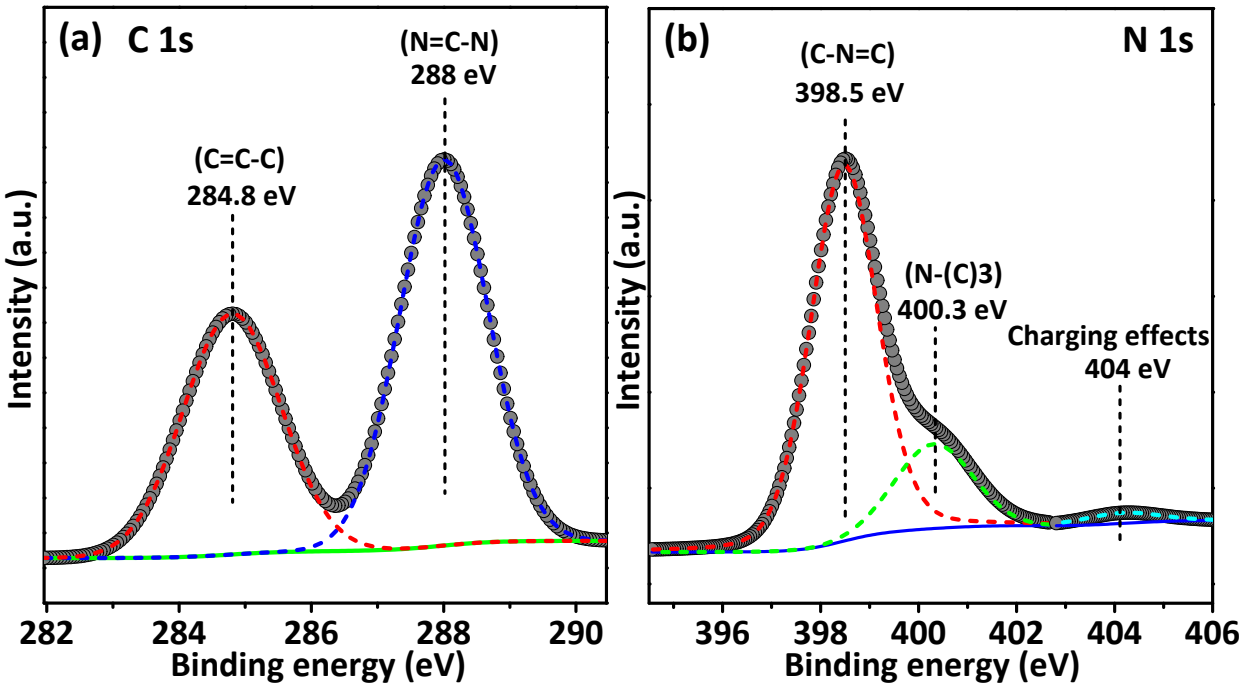

Fig. S8 The high-resolution XPS spectra of (a) C 1s and (b) N 1s for PCN-S.

Fig. S8a and b show the high-resolution XPS spectra of C 1s and N 1s for PCN-S. The C 1s spectrum of PCN-S was deconvoluted into two components. The dominant peak at 288 eV is assigned to sp^2 bonded carbon in N-containing aromatic rings (N=C-N).[1] And the peak at 284.8 eV corresponds to the sp^2 C-C bonds.[1] Moreover, the N 1s spectrum of PCN-S can be fitted with three contributions located at 398.5 eV, 400.3 eV and 404 eV, which are ascribed to sp^2 bonded nitrogen in N-containing aromatic rings (C-N=C), tertiary nitrogen (N-(C)3) and charging effects or positive charge location.[2]

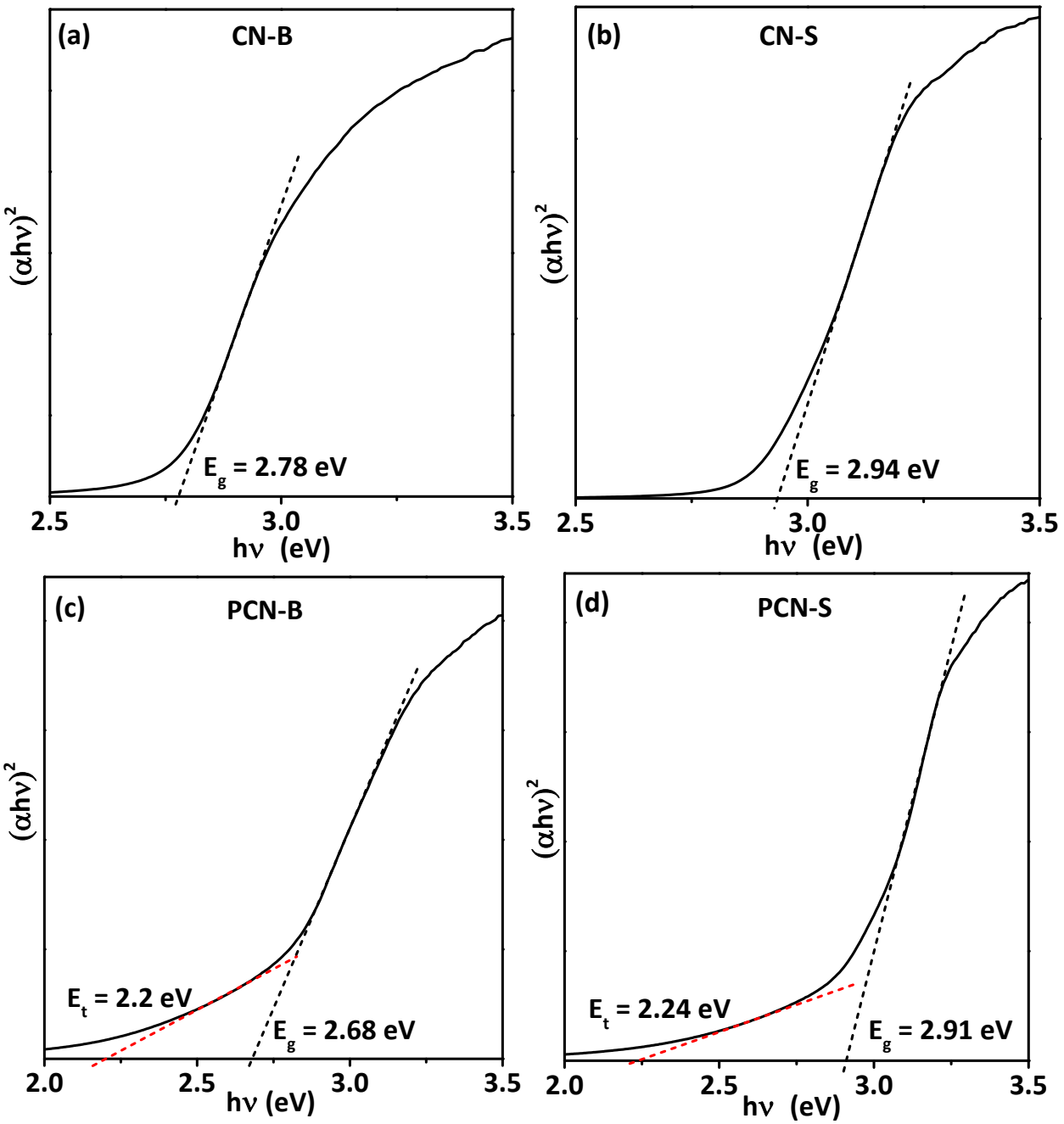

Fig. S9 The band gap energy (E_g) for (a) CN-B and (b) CN-S; the band gap energy (E_g) and transition energy (E_t) from VB to the midgap states for (c) PCN-B and (d) PCN-S.

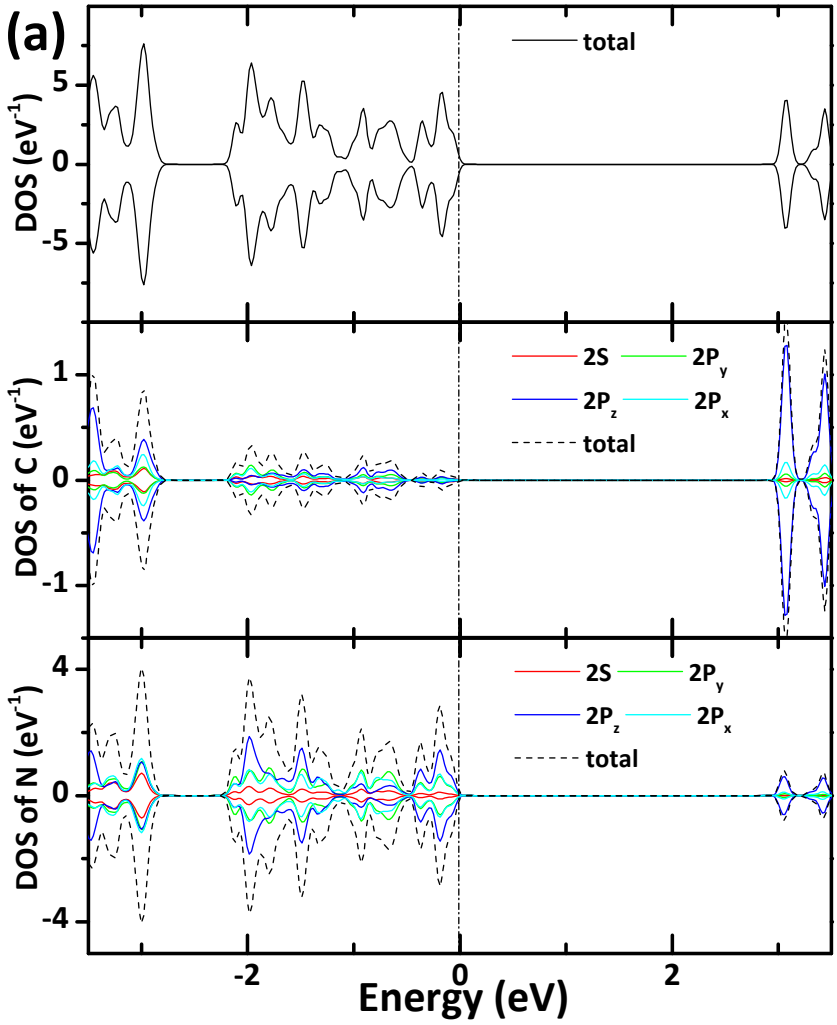

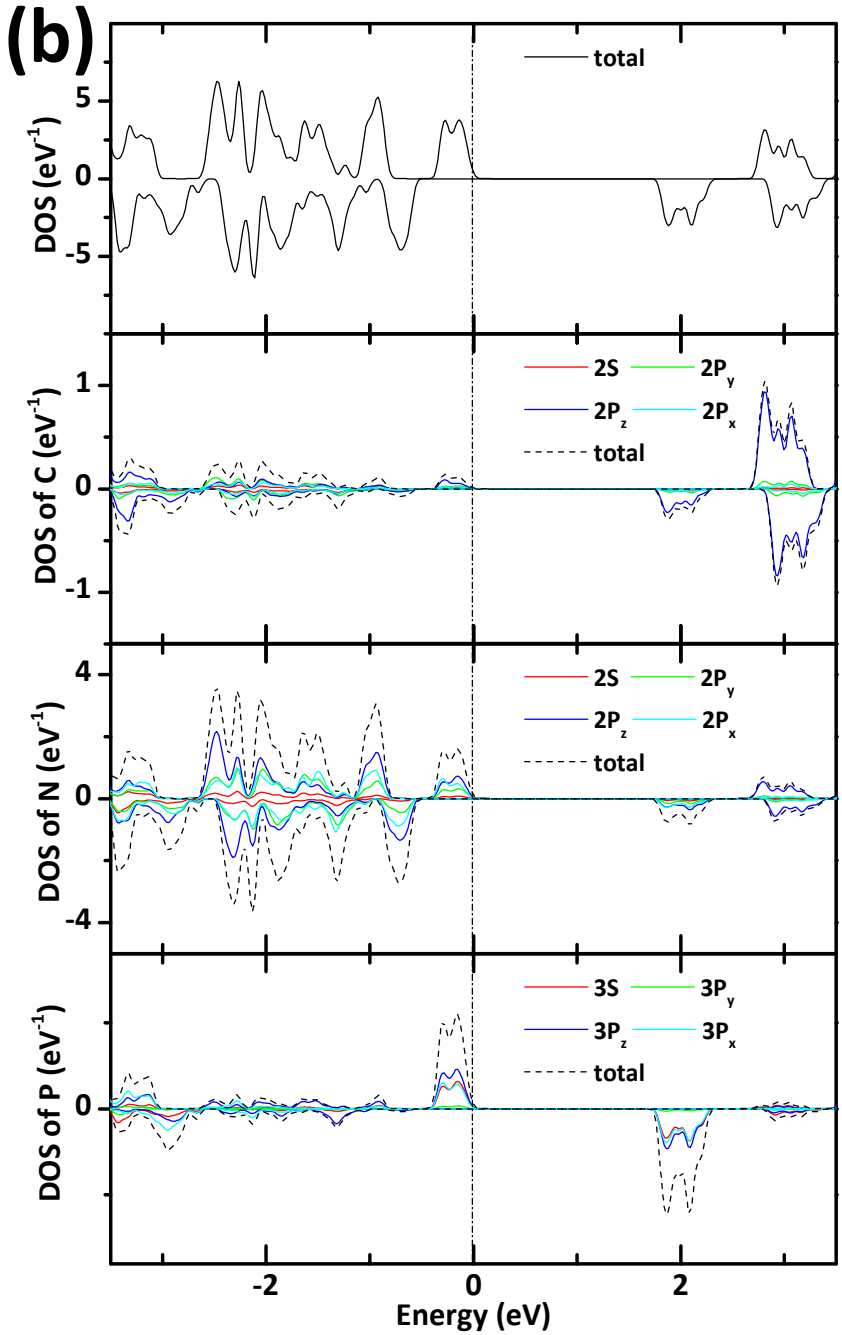

Fig. S10 TDOS and PDOS of (a) pure g-C_3N_4 and (b) P-doped g-C_3N_4. The Fermi level is set to the zero of energy.

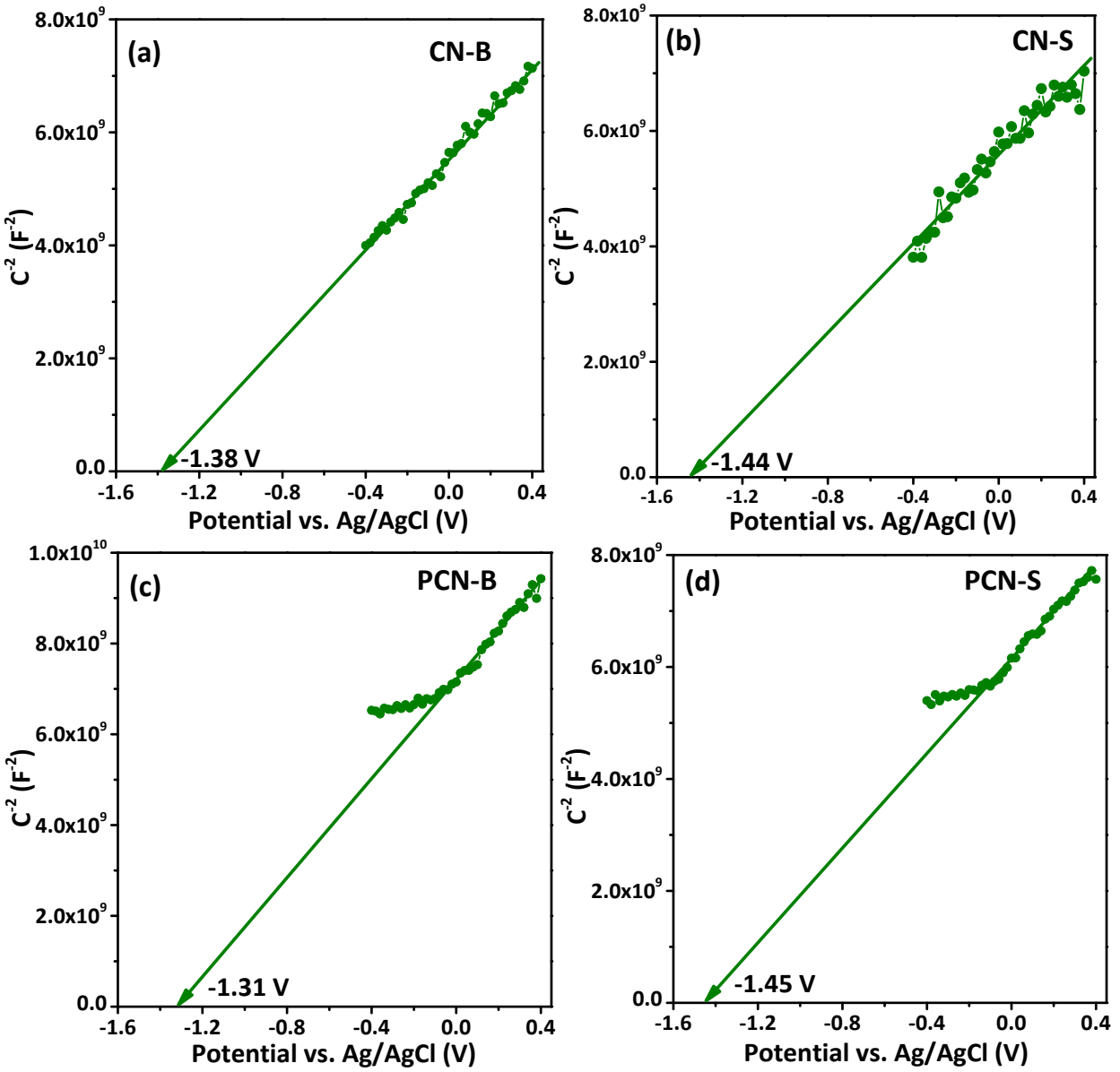

Fig. S11 Mott-Schottky plots of (a) CN-B (b) CN-S (c) PCN-B and (d) PCN-S in 0.2 M Na_2SO_4 aqueous solution.

As presented in Fig. S11a-d, the flat band potentials of CN-B, CN-S, PCN-B and PCN-S are determined to be at -1.38 V, -1.44 V, -1.31 V and -1.45 V *vs.* Ag/AgCl at pH = 6.6, which correspond to -0.76 V, -0.82 V, -0.69 V and -0.83 V *vs.* SHE at pH = 0, respectively.

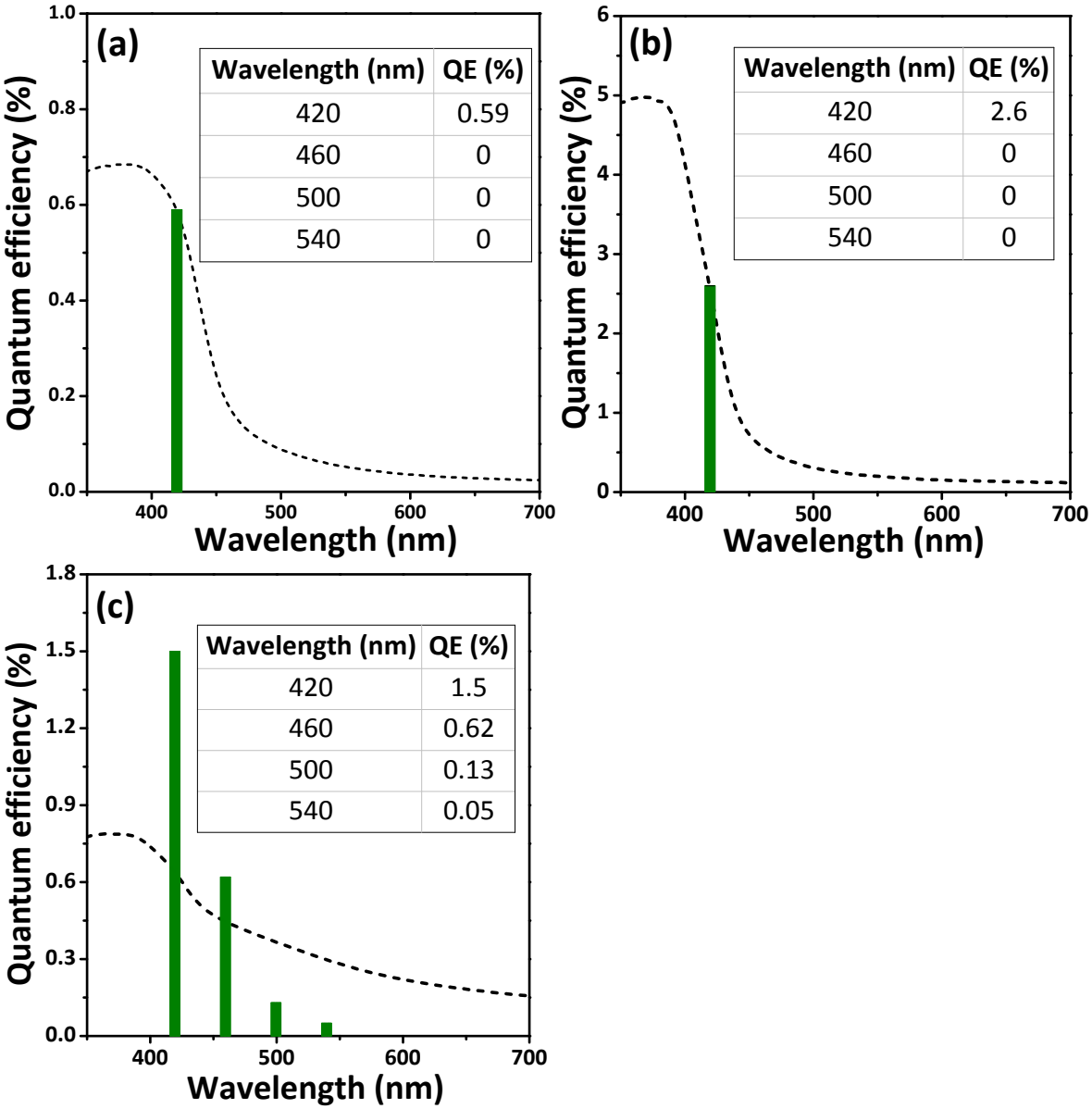

Fig. S12 QE of (a) CN-B, (b) CN-S and (c) PCN-B at 420 nm, 460 nm, 500 nm or 540 nm, respectively.

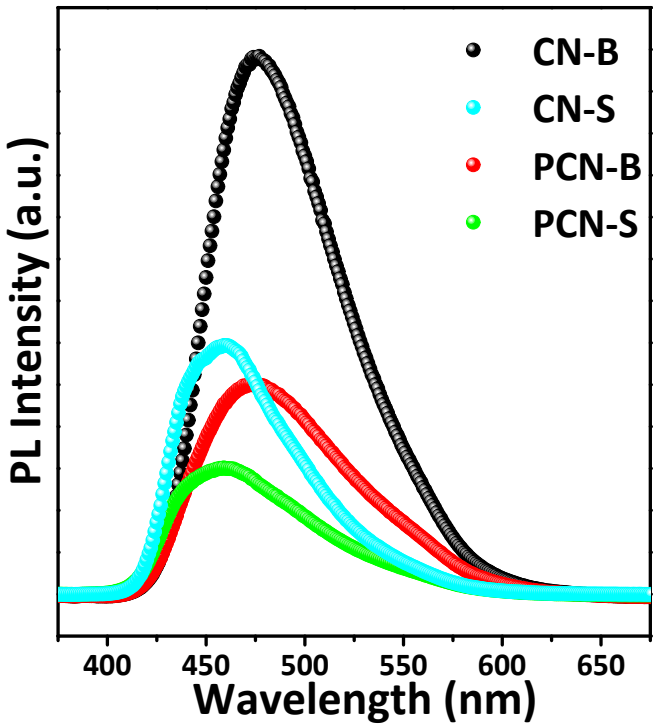

Fig. S13 Steady-state PL spectra of CN-B, CN-S, PCN-B and PCN-S at 350 nm excitation light.

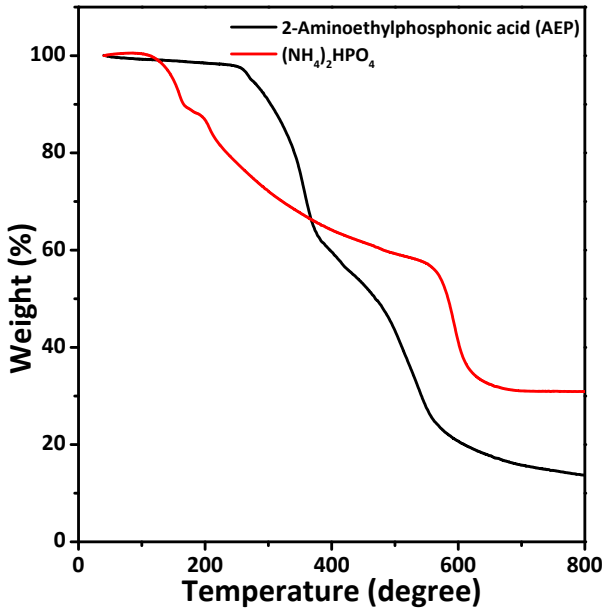

Fig. S14 TG curve of 2-aminoethylphosphonic acid (AEP) and $(NH_4)_2HPO_4$.

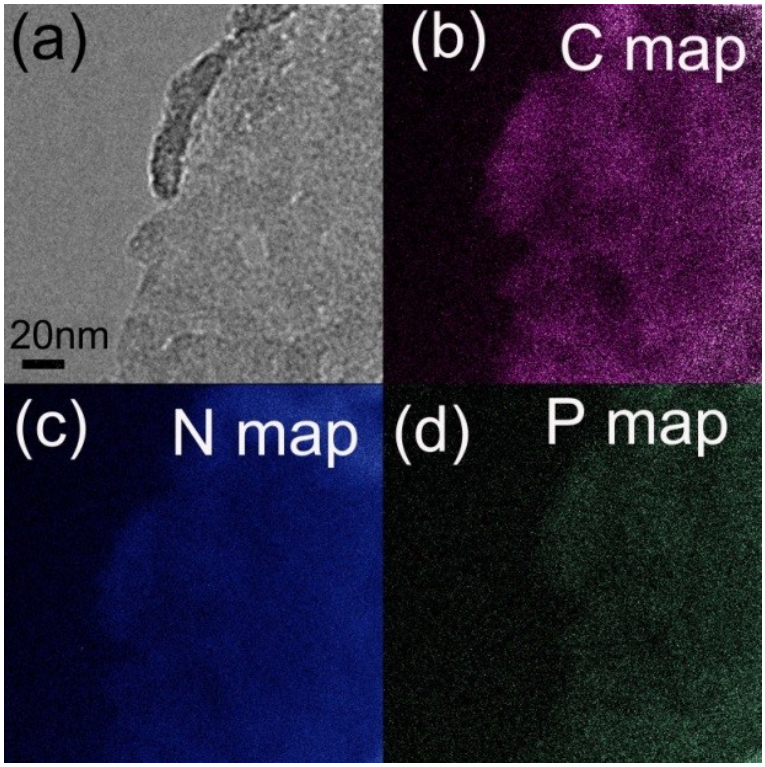

Fig. S15 TEM image (a) of PCN-S and its corresponding EELS elemental mapping images (b-d).

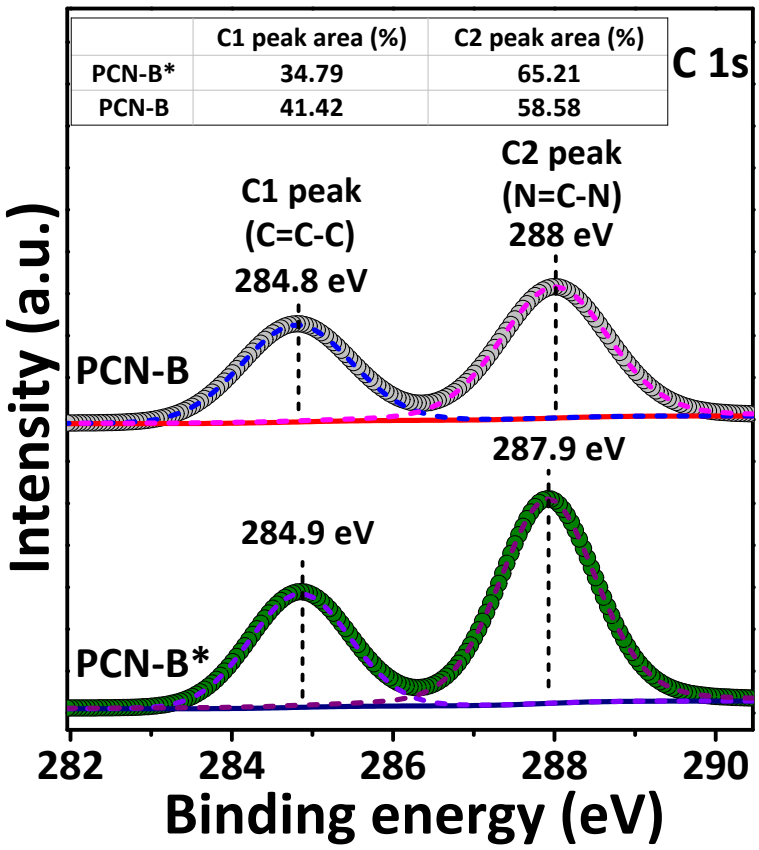

Fig. S16 The high-resolution XPS spectra of C 1s for PCN-B and PCN-B*. The table in **Fig. S16** shows the C1 and C2 peak area percentages for PCN-B and PCN-B*, respectively.

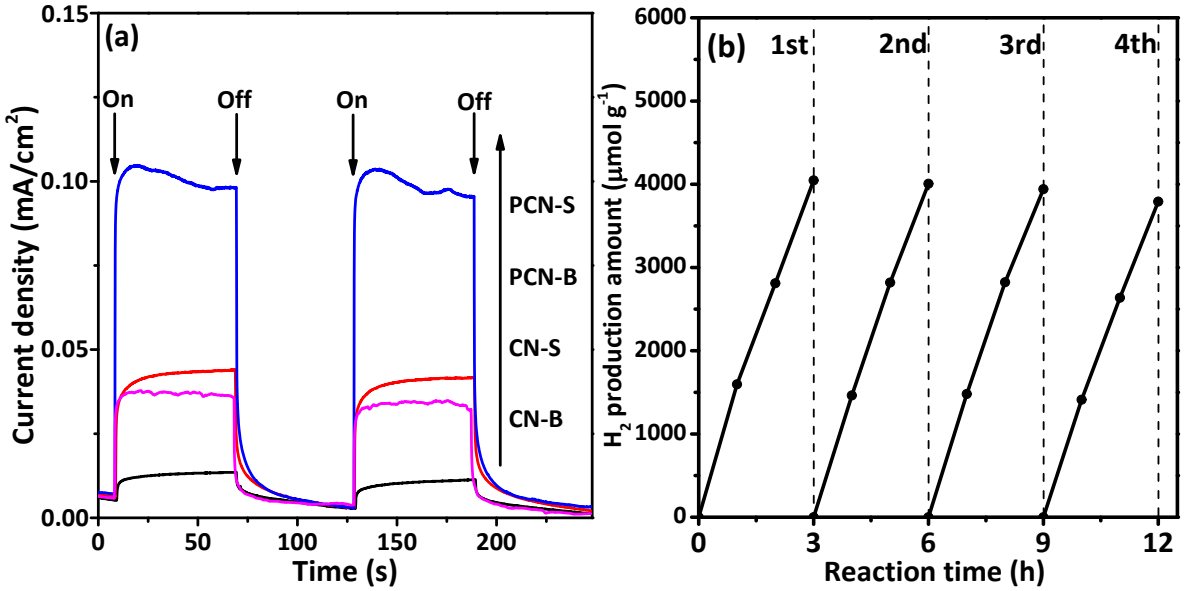

Fig. S17 (a) TPC responses of CN-B, CN-S, PCN-B and PCN-S electrodes in 0.2 M Na_2S + 0.04 M Na_2SO_3 mixed aqueous solution under visible-light irradiation and (b) Time course of photocatalytic H_2-production over sample PCN-S. The reaction system is purged with Ar every three hours for 30 min to remove the H_2 inside.

References

1. G. Zhang, J. Zhang, M. Zhang and X. Wang, *J. Mater. Chem.*, 2012, **22**, 8083.

2. A. Thomas, A. Fischer, F. Goettmann, M. Antonietti, J.-O. Muller, R. Schlogl and J. M. Carlsson, *J. Mater. Chem.*, 2008, **18**, 4893.